RESEARCH ARTICLE

Space-based Earth remote sensing: Part 1. Satellite orbit theory

Sung Wook Paek[1], Sangtae Kim[2]

[1] Department of Aeronautics and Astronautics, Massachusetts Institute of Technology

[2] Department of Material Science and Engineering, Massachusetts Institute of Technology

[*] Correspondence to: Sung Wook Paek, Email: paek@alum.mit.edu

Abstract: The development of oceanography and meteorology has greatly benefited from remotely sensed satellite data of the atmosphere and ocean. For oceanographers, meteorologists, hydrologists and climatologists to obtain high-quality satellite data, orbits along which the satellites move must be designed carefully. For this reason, Sun-synchronous, repeat ground track orbits have traditionally been used for visible-wavelength and infrared Earth observations. As the needs for varied datasets are growing, however, new classes of Earth-observing missions are emerging such as interferometry and radiometry to name a few. On the other side, satellite platforms and onboard sensors are getting more compact and less expensive, allowing developing nations to launch their own satellites and under-researched parts of the Earth be studied. In light of these changes, this paper introduces new types of satellite orbits from celestial mechanics perspectives, whose applications will be detailed further in the follow-up work.

Keywords: satellite orbit; Sun-synchronous orbit; repeat ground track; quasi-synchronization; tide

1. Introduction

Space-based remote sensing has played a crucial role in studying our planet Earth. The LandSat Program, the longest-operating Earth observation mission since 1972, had a primary goal of imaging the Earth's landmass and capturing the changes therein[1]. SeaSat, launched in 1978, was the first satellite dedicated to ocean research[2]. During its 105-day lifetime, SeaSat could acquire more information than collected by shipboard surveys for the preceding 100 years[3]. The measurement data from the Earth Radiation Budget Satellite (ERBS) led to the finding of stratospheric ozone depletion over the Polar Regions[4]. The ensuing global decision-making process has culminated in the Montreal Protocol which is considered the most successful climate agreement in history. Meteorological satellites are also launched in constellations as illustrated by NASA's A-train. The satellites are placed in series a few minutes apart from each other, enabling the construction of three-dimensional representations of both ground surface and atmosphere[5]. For instance, the Aqua satellite gathers information of water with all phases in atmosphere, cryosphere, land and oceans to study the water cycle of the Earth[6]. CloudSat in the same train is the first satellite that characterizes the vertical structure of clouds, whose data can then be assimilated into current atmospheric models to better predict weathers and climate changes[7]. The A-train is also the product of joint multi-national efforts by the United States, Canada, United Kingdom, France, Japan and Brazil.

The first-generation weather satellites used non-polar (i.e. low inclination) low-Earth orbits (LEOs) as illustrated by Television and Infrared Observation Satellites (1960). Since the second generation marked by the Nimbus series (1964), near-polar (i.e. high inclination) Sun-synchronous orbits have become the norm in Earth remote sensing[8].

doi: 10.18063/som.v3i1.646

Satellites in Sun-synchronous orbits (SSOs) cross a given latitude band at the same mean local time (MLT) throughout a year, providing uniform illumination conditions in visible or infrared wavelengths. On the other side, satellites performing radio-frequency measurements do not benefit from Sun-synchronization and thus do not require SSOs. NASA's recent Cyclone Global Navigation Satellite Mission (CYGNSS), launched in 2016, is observing GPS signals reflected from the oceans to measure wind speeds in an orbit with a 35° inclination angle and a 500km altitude[9]. The Sentinel-6 satellite, planned for a launch by the European Organisation for Metrological Satellites (EUMETSAT) in the 2020-2030 time frames, will use radar signals for precision ocean altimetry and be in a non-SSO with a 1336km altitude and a 66° inclination angle[10].

An SSO, sometimes termed the helio-synchronous orbit, has an orbit inclination between 96.5° and 102.5°, close to a polar orbit with an inclination of 90°[11, 12]. Therefore, SSOs can provide global coverage at nearly all latitudes. Year-round uniform lighting conditions for observed targets are essential in comparison of satellite images taken at different times of a year. Uniform solar illuminating angles also help satellites maintain constant thermal conditions for themselves and their onboard sensors. The SSOs can further be designed to have repeat ground tracks (RGT) such that targets near the periodically repeating paths are observed more frequently.

Following the brief history of spaceborne Earth observation introduced here, Chapter 2 revisits basic terminology used to characterize satellite orbits. Based on these nomenclature and definitions, Chapter 3 continues in-depth discussion of widely-used Earth-observing orbits such as SSOs and RGT orbits while proposing new applications for non-RGT orbits. Chapter 4 further expands these types of orbits by incorporating novel concepts such as quasi-Sun-synchronous RGT orbits and tidal-synchronous RGT orbits. Chapter 5 summarizes the paper with conclusions and future research.

2. Satellite Orbit Basics for Earth Remote Sensing

Unlike airborne remote sensing that provides limited spatiotemporal coverage during flight, spaceborne remote sensing offers more regular and global coverage from perpetually revolving orbits in space. The orbit of an Earth-observing satellite is described using six parameters or orbital elements: a, e, i, Ω, ω, ν[13]. The first two elements define the size and shape of an orbit: semi-major axis (a) for size and eccentricity (e) for shape. The next two elements define the three-dimensional orientation of an orbit. Inclination (i) defines the tilting angle of a satellite's orbit plane with respect to the Earth's equator, and the longitude of the ascending node (Ω) defines the tilting nodes location measured from the vernal equinox position. For an Earth-centered orbit, the longitude of the ascending node is also referred as the right ascension of the ascending node (RAAN). From the ascending node, the argument of perigee (ω) is measured, from which the satellite's position is determined with the true anomaly (ν). Due to the satellite's motion, the anomaly is defined as the angular position at a specific moment in time, or "epoch."

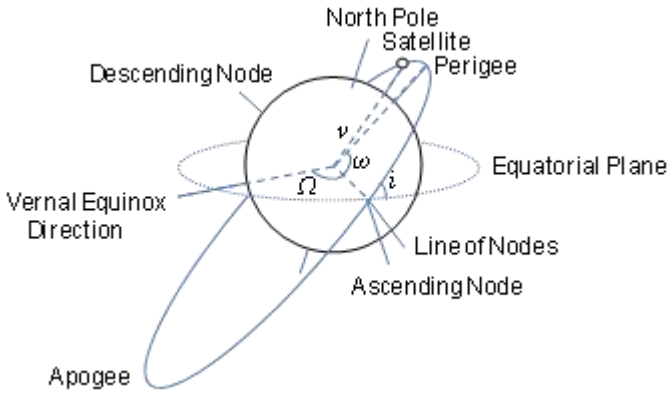

Figure 1. Nomenclature of an Earth-centered orbit.

Of practical interest to oceanographers and meteorologists is the areal coverage that can be achieved by space-based remote-sensing systems. The projection of a satellite's orbit on the Earth's surface towards the Earth's center marks a path or trace, usually called a ground track. **Figure 2** depict two types of ground tracks: repeating and non-repeating[14,15]. The repeat ground track returns to its starting point after a certain period, usually several days or weeks. Because of this periodicity, ground locations near the path can be observed more frequently. In particular, intersections of traces in **Figure 2** (A) are locations observable both at the ascending node and at the descending node shown in **Figure 1.** On the other hand, locations between paths are inaccessible and left as dead zones. The non-repeat ground track does not repeat itself and is spread over the entire globe as shown in Figure 2 (B). A specific target is observed less frequently, but all places are given equal observation opportunities without dead zones.

Finally, the symbol in each map is the point on the Earth's surface beneath the satellite (sub-satellite point). The wider a satellite sensor's field of view (FOV) is, the more area around the sub-satellite point can be observed at once[16–18]. The dark shaded area in each map represents regions where the sunlight cannot reach. Maintaining the same solar local time (solar elevation) at each observation opportunity is crucial for Earth observation in visible or infrared wavelengths, leading to the concept of Sun-synchronous orbits.

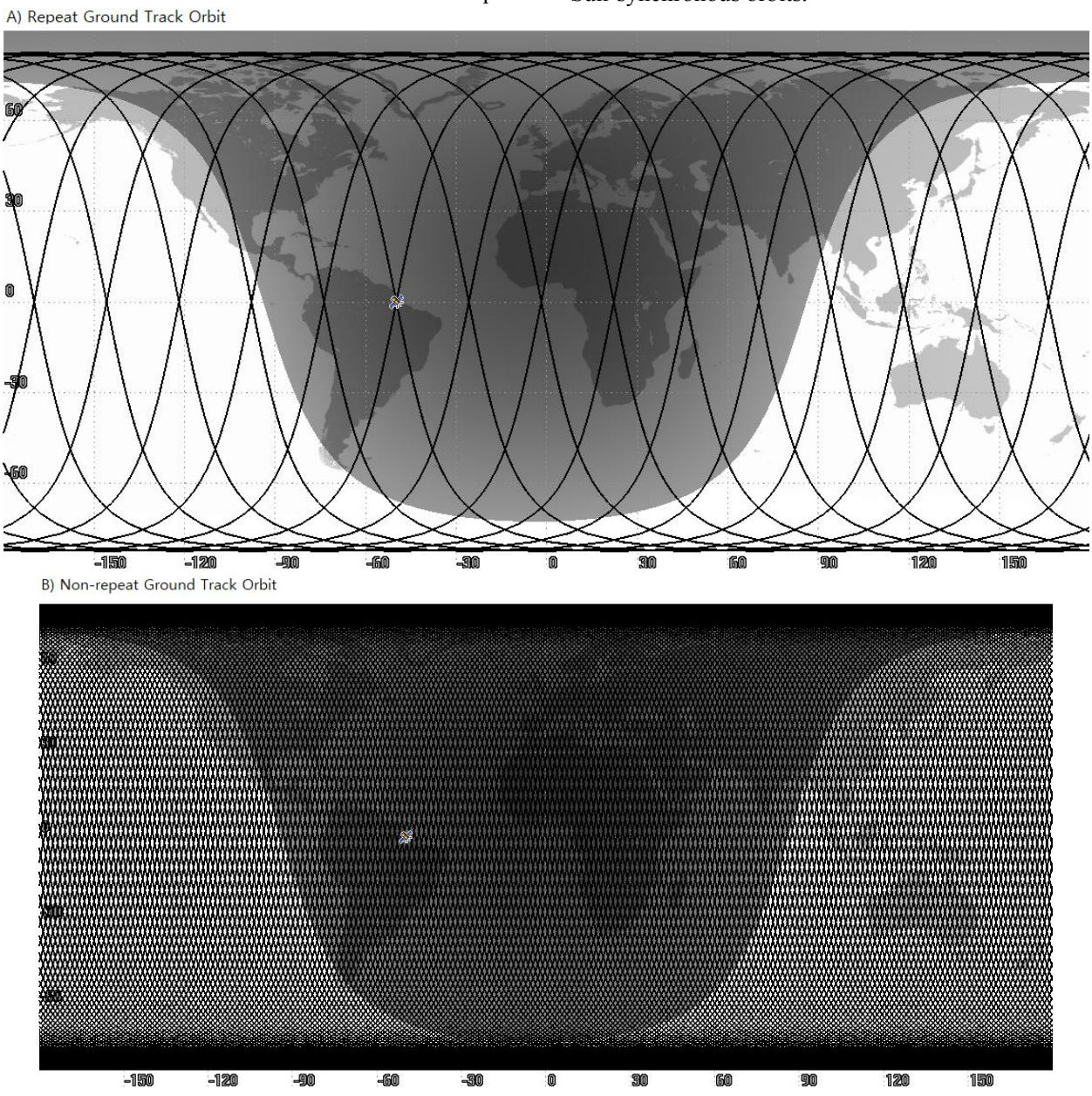

Figure 2. Repeat ground track (A) and non-repeat ground track (B) of Sun-synchronous orbits with same inclination angles (97.63°) and differing altitudes (561 km for A and 583 km for B).

3. Sun-synchronous Orbits and Repeat Ground Track Orbit

In terms of orbital elements, the inclination of Sun-synchronous orbits (SSOs) is confined within a narrow range between 96.5° and 102.5°. Observation opportunities are further limited for SSOs to also have repeat ground tracks. An SSO may have non-repeating, drift ground tracks whose ground speed is matched with moving targets such as typhoons.

3.1 Sun-synchronous Orbits

The Earth's equatorial radius is greater than its polar radius due to its spin and equatorial bulge. The torque exerted by the extra equatorial mass causes a satellite orbit to precess (i.e. nodal regression). This is similar to a phenomenon where a spinning top wobbles due to gravitational forces. When the satellite orbit precesses, the satellite visits a given latitude band at different local sidereal times, as illustrated by the non-fixed, low-inclination orbit in **Figure 3**(A). Complete elimination of nodal regression, however, is not useful for Earth observation either. The polar (i.e. i = 90°) orbit in **Figure 3**(A) illustrates a case where the nodal regression is set to zero and the orbit is fixed in the inertial frame. Although the local "sidereal" time now remains the same throughout a year, the local "solar" time varies according to the Earth's position relative to the Sun. **Figure 3** shows that the local time of observation is dawn or dusk in summer and winter, noon or midnight in spring or autumn. To provide uniform solar illumination for satellite imaging, the nodal regression should match the Earth's yearly revolution rate around the Sun, not zero.

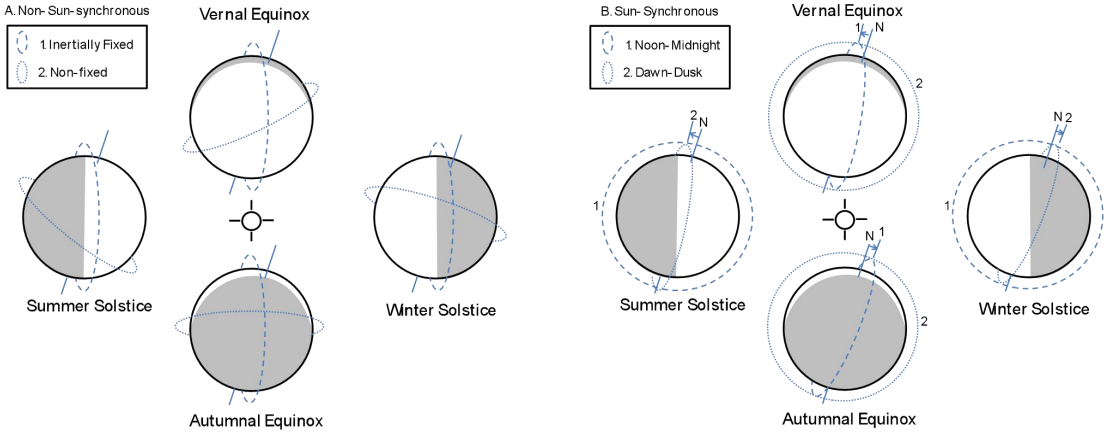

Figure 3. Satellite orbits that are not Sun-synchronous (A) and Sun-synchronous (B). Orbits not synchronized with the Sun may have too low (A-1) or too high (A-2) nodal regression rates. Orbits synchronized with the Sun have the nodal regression rate equal to the Earth's yearly revolution around the Sun with varied constant RAAN values (B-1, B-2).

Equation (1) gives the satellite orbit's regression, which should be equal to 360° ÷ 365.2422 day = 0.9856°/day = 2×10^{-7} rad/s. In Eq. (1), $d\Omega/dt$ is the nodal regression rate which is the time derivative of the longitude of the ascending node Ω (RAAN). It is a function of semi-major axis (a), eccentricity (e) and inclination (i). The remaining symbols are all constants; R_E is the Earth's equatorial radius, J_2 is the Earth's oblateness coefficient (1.08263×10^{-3}) and μ_E is the Earth's standard gravitational parameter (3.986×105 km^3s^{-2}). **Figure 4** illustrates Sun-synchronous orbits with $d\Omega/dt$ = 0.9856°/day. Depending on initial values of Ω which determine a satellite's passage time over a target, a SSO can be named as a noon-midnight orbit, a dawn-dusk orbit, a 10:30 AM/PM orbit, etc.

$$\dot{\Omega} = -\frac{3R_E^2 J_2 \sqrt{\mu_E}}{2a^{7/2}(1-e^2)^2}\cos(i) \qquad (1)$$

Figure 4 is a plot of the nodal regression rate which is a function of semi-major axis and inclination. The eccentricity is zero and constant under the circular orbit assumption. The curved surface is the nodal regression rate and the flat plane is where $d\Omega/dt$ = 0.9856°/day holds. Consequently, the intersecting line between the two surfaces consists of (a, i)-pairs

that all satisfy Sun-synchronous conditions[18]. By incrementing e to positive values and stacking the intersecting lines will result in a three-dimensional (a, e, i)-surface for all Sun-synchronous orbits[13]. If the eccentricity grows large, the minimal distance from the satellite to the Earth surface will vary between its apogee and its perigee, resulting in uneven variation in data resolution. Hence, this paper only considers circular orbits for both simplicity and practicality.

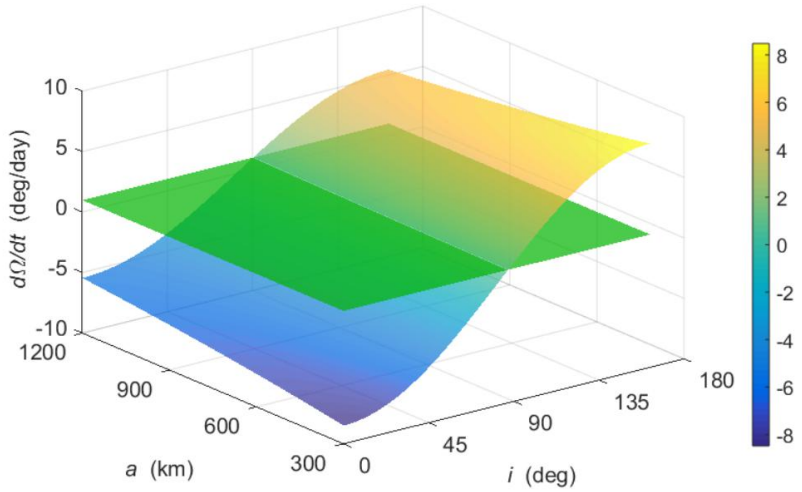

Figure 4. Dependence of the orbit nodal regression rate (deg/day) on semi-major axis (a) and inclination (i) with zero eccentricity (e = 0). The intersecting line with the plane (dΩ/dt = 0.9856°/day) defines the orbital elements of circular SSOs.

3.2 Repeat Ground Track Orbits

An orbit has repeat ground tracks (RGTs) if a satellite's ground track exactly repeats its pattern after a certain period of time, usually specified in days. With an Earth nodal period T_N and a satellite orbital period T_S, the satellite will complete N_S revolutions around the Earth after N_D nodal days.

$$N_S T_S = T_N N_D \quad (2)$$

Rearranging Eq. (2) and substituting the definitions of T_N and T_S, Eq. (3) can be obtained[19]. We define the RGT ratio τ such that its value is greater than 1 for orbits within the geostationary orbit ($\tau = 1$), which is mostly the case in Earth observations. For example, a satellite whose orbit has $\tau = 15$ will orbit the Earth 15 times a day with a period of 96 minutes. For $\tau = 14.5 = 29/2$, a satellite will orbit the Earth 29 times in two days, at a slightly slower rate, resulting in a longer period of 99 minutes. Dividing 2π by this orbital period equals $n = (\mu_E/a^3)^{1/2}$ in Eq. (3) referred to as the mean motion. The perturbation of the mean motion due to the Earth's oblateness is denoted as Δn and is given in Eq. (4). For an elliptical orbit in which $e > 0$, the argument of perigee also precesses due to perturbation, which is defined as $d\omega/dt$ in Eq. (5). The spin rate of the Earth ω_E is a constant term equal to $360° \div 1$ day $= 7.29 \times 10^{-5}$ rad/s.

$$\tau = \frac{N_S}{N_D} = \frac{T_N}{T_S} = \frac{2\pi/(\omega_E - \dot{\Omega})}{2\pi/(\dot{M} + \dot{\omega})} = \frac{n + \Delta n + \dot{\omega}}{\omega_E - \dot{\Omega}} \quad (3)$$

$$\Delta n = \frac{3R_E^2 J_2 \sqrt{\mu_E}}{4a^{7/2}(1-e^2)^{3/2}}(2 - 3\sin^2 i) \quad (4)$$

$$\dot{\omega} = \frac{3R_E^2 J_2 \sqrt{\mu_E}}{4a^{7/2}(1-e^2)^2}(4 - 5\sin^2 i) \quad (5)$$

It is possible for an RGT orbit to be Sun-synchronous at the same time. Setting $d\Omega/dt = \omega_{ES} = 0.9856°$/day and $e = 0$ in Eqs. (1), (3), (4) and (5) yields Eq. (6) which is a formula for circular Sun-synchronous repeat ground track (SSRGT) orbits.

$$\sqrt{\frac{\mu_E}{(R_E+h)^3}} + \frac{J_2 R_E^2 \sqrt{\mu_E}}{(R_E+h)^{7/2}}\left(\frac{8}{3}\frac{(R_E+h)^7 \omega_{ES}^2}{J_2^2 R_E^4 \mu_E} + \frac{3}{2}\right) + (\omega_E - \omega_{ES})\tau = 0 \quad (6)$$

Fixing the $d\Omega/dt$ value and letting $e = 0$, there are only two variables a and i remaining in Eq. (1). Therefore, an SSRGT orbit's inclination i is the function of the semi-major axis $a = R_E + h$ only, where h is the orbit altitude. Similarly, h is the function of RGT ratio τ only as can be seen in Eq. (6). This one-to-one relationship among inclination, altitude and RGT ratio (i.e. repeat cycle N_D and number of periods N_S) are depicted in **Figure 5**[14,18].

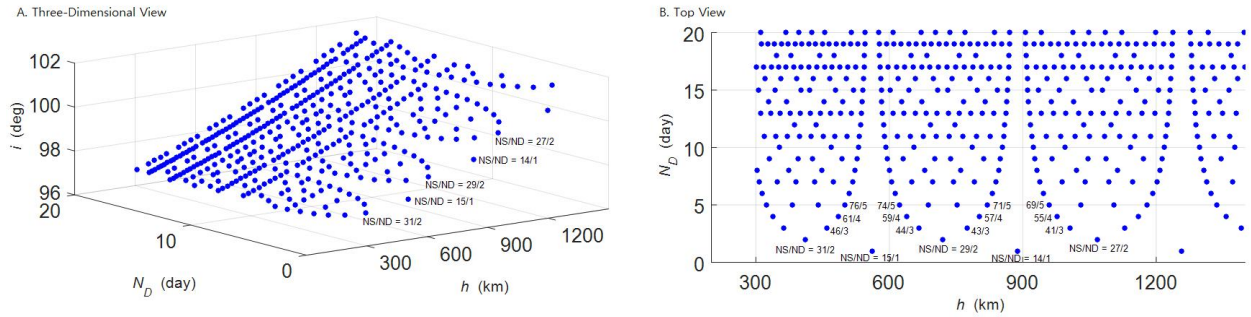

Figure 5. SSRGT orbit altitude and inclination in (A) 3-dimentional view and (B) top view.

3.3 Drift Ground Track Orbits

Although a drift ground track (DGT) orbit can be seen simply as all non-RGT orbits, this paper uses the term DGT to emphasize that ground tracks are drifted by design for remote-sensing purposes. The ground tracks of an RGT orbit and a DGT orbit are compared in **Figure 1.** Unlike the fixed ground track of an RGT orbit which repeats after a certain period of time, the ground track of a DGT orbit will appear drifting eastward or westward relative to its RGT reference. The RGT orbit in Figure 1(A) has the RGT ratio of 15 at the 561 km altitude, meaning that a satellite in this orbit will return to the original starting position after 1 day or 15 revolutions. If the satellite altitude is decreased to 500 km, the satellite's location after the same time interval will be 500 km east to the starting point, corresponding to a drift speed of 20 km/h. It is assumed that the satellite's initial location was at the equator. The drifting of ground tracks comes from the difference in orbital periods between a RGT orbit and a DGT orbit. If the semi-major axis of the non-RGT orbit deviates from that of a RGT orbit by δa (or orbital height differs by δh, the periodic difference is given by Eq. (7).

$$\delta T = 2\pi\left(\sqrt{\frac{(a+\delta a)^3}{\mu_E}} - \sqrt{\frac{a^3}{\mu_E}}\right) \quad (7)$$

If δa > 0, the DGT orbital period increases; its ground track drifts westward because the DGT is lagging the corresponding RGT. If δa < 0, the DGT with a shorter period will lead the counterpart RGT, drifting eastward. The drift distance per orbit at the equator is the product of the period difference and the Earth's rotation speed. The effective instantaneous velocity can be expressed as δa/δT.

$$\delta d = \left(\omega_E - \dot{\Omega}\right) R_E \delta T \quad (8)$$

Figure 7 shows the relationship between |δa/δT| and δh calculated at select reference altitudes. It is noteworthy that the drift velocity has very similar slopes for different RGT ratios. The plot shows RGT altitudes ranging between 400 km and 700 km, but this tendency applies to wider altitude ranges as well. The instantaneous drift rate of a ground track increases by approximately 0.3 km/h as the satellite is placed one kilometer farther from the baseline RGT altitude, which can be matched to the speed of mobile targets in the atmosphere or oceans such as hurricanes or glaciers. The resolution of satellite imagery is maximized when the distance between a satellite and a target is minimized. Therefore, matching the sub-satellite point as closely with the mobile target's time-varying location as possible will improve the quality of satellite data. Table 1 summarizes the ground speed statistics of Atlantic hurricanes. The data spans a time period between 1851 and 2014, obtained from the National Hurricane Center's North Atlantic hurricane database[20]. Over 70% of the cases during this period were observed between 10°N and 30°N, whose ground speed is about 20 km/h. This speed corresponds to the difference δa = δh = 50 km. Of course, tropical storms continually change their ground speed and direction throughout development stages; even if the ground speed is constant, the changing of forward directions will alter the value of δd because it is the latitudinal projection parallel to the equator. The combination of both speed and direction changes would require frequent accelerating or decelerating maneuvers, which is unrealistic from a satellite operational point of view. Acceleration or deceleration of the ground track speed requires lowering or raising altitudes, which consumes extra fuel in addition to regular orbital maintenance. The regular orbit-maintaining routines include readjustment of orbit elements with impulse fuel burns to counteract external perturbations, such as atmospheric friction or solar radiation pressure, before the unintended orbital changes grow beyond reversible

limits. When a satellite uses up its fuel for orbital maintenance, the satellite loses its control over its orbit. Once a satellite orbit becomes no longer Sun-synchronous, the value of satellite imagery will be lost. Because satellites cannot be refueled in orbit with our current technology, additional maneuvers to match the target speed are detrimental to a satellite's useful life. A more realistic option would be to deploy a fleet of satellites with a preset drift speed for each of them. Each satellite cannot readjust its ground drift speed, but at least one of the entire fleet will closely match the ground speed of the target of interest. Several projects have been proposed to launch small satellites to construct a constellation for global monitoring of tropical storms[21,22]. Use of multiple DGTs with a ground speed distribution will be further analyzed in the future work.

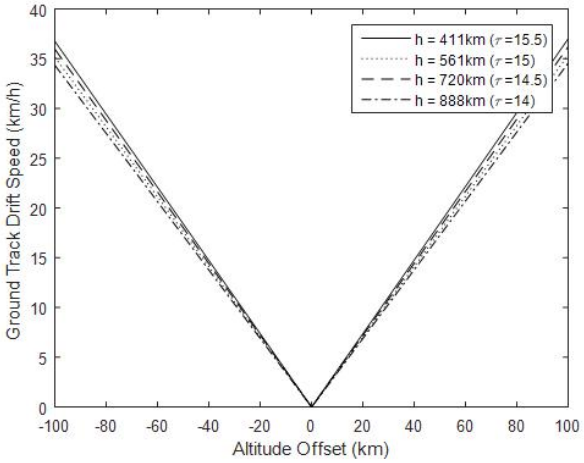

Figure 6. Forward speed of drifting ground track.

Latitude	Speed	No. Cases
0 – 5 °N	25.9 km/h (16.1 mph)	186
5 – 10 °N	22.0 km/h (13.7 mph)	4678
10 – 15 °N	19.2 km/h (11.9 mph)	7620
15 – 20 °N	17.4 km/h (10.8 mph)	7501
20 – 25 °N	17.5 km/h (10.8 mph)	8602
25 – 30 °N	20.1 km/h (12.5 mph)	6469
30 – 35 °N	27.1 km/h (16.9 mph)	3397
35 – 40 °N	39.0 km/h (24.2 mph)	1120
40 – 45 °N	49.3 km/h (30.6 mph)	264

Table 1. Forward speed of Atlantic hurricanes averaged by 5 degree latitude intervals.

4. Quasi-Sun-Synchronous Orbits and Tidal Synchronous Orbits

As shown in Chapter 3, Sun-synchronous orbits have narrow ranges for orbital elements. To overcome this limitation, the definition of SSOs can be extended to include quasi-SSOs. It is also possible to synchronize satellite orbital periods with the Moon instead of the Sun, resulting in tidal synchronous orbits (TSOs).

4.1 Quasi-Sun-synchronous Orbits

Because SSOs are nearly polar (i $\approx$ 90°), they provide near-global spatial coverage as shown in **Figure 1** and **Figure 2.** However, the temporal coverage of an SSO is not uniform (Paek *et al*, 2012). Ground tracks are more densely populated near poles than near the equator, meaning that satellites can view Polar Regions more often than equatorial regions. Inclination i must be decreased to move the ground track "bundles" closer to the equator and to observe equatorial regions more often, but then the orbit will no longer be Sun-synchronous. This problem may be circumnavigated by loosening the definition of SSOs. By its narrow definition, an SSO provides the uniform

solar elevation angle all the time at every location. One of possible broader definitions is to enforce Sun-synchronization only at specific locations and times. The idea of quasi-SSOs or "multi-SSOs" was proposed by Bruccoleri *et al*. (2004)[23], and this paper further analyzes their RGT characteristics. As seen in Figure 5, it is possible to boost the nodal regression rate dΩ/dt beyond ω_{ES} = 0.9856°/day. If we denote this extra increment by $\Delta\omega_{ES}$, the new inclination and altitude values can be found from Eq. (9).

$$\sqrt{\frac{\mu_E}{(R_E+h)^3}}+\frac{J_2R_E^2\sqrt{\mu_E}}{(R_E+h)^{7/2}}\left(\frac{8}{3}\frac{(R_E+h)^7(\omega_E+\Delta\omega_{ES})^2}{J_2^2R_E^4\mu_E}+\frac{3}{2}\right)+(\omega_E-\Delta\omega_{ES}-\omega_{ES})\tau=0 \quad (9)$$

Because of trigonometric functions used in the dΩ/dt expression, the maximum value of ΔωES is limited to slightly more than 8°/day. There is no real solution for altitude and inclination for accelerating dΩ/dt by more than this threshold. Assuming $\Delta\omega_{ES}$ = 6°/day and τ = 15, the orbit is Sun-synchronous and has repeat ground tracks every 60 days. During this period, the orbital node precesses by (0.9856°/day + 6°/day) × 60 day, where the second term vanishes after modulus operation (mod 360°). With the boost term, the inclination of quasi-Sun-synchronous orbits covers a much broader range as shown in **Figure 8.** A strictly Sun-synchronous orbit had an altitude of 561 km and an inclination of 97.64° inclination for τ = 15, as marked in Figure 6(A). With $\Delta\omega_{ES}$ = 6°/day, the same repeat ratio results in a quasi-Sun-synchronous orbit with a 663 km altitude and a 172.4° inclination which is nearly equatorial. For τ = 16, a strict SSO has an altitude below 300 km which is considered too low to sustain the satellite altitude because of atmospheric drag; a corresponding quasi-SSO have a 362 km orbit and a 148.3° inclination. The plateau in Figure 8 at higher altitudes is a keep-out zone where the inclination contains an imaginary part and thus quasi-SSOs cannot exist. All feasible solutions in Figure 7(A) require 60 days for quasi-SSRGT orbits to have the same sub-satellite point location and the same solar time with SSRGT orbits.

If $\Delta\omega_{ES}$ is negative, the magnitude $|\Delta\omega_{ES}|$ can be further increased, reducing the number of days required for synchronization with SSRGT orbits. For $\Delta\omega_{ES}$ = -9°/day, a quasi-SSRGT orbit with τ = 15.5 have an altitude of 323 km and a 17.0° inclination. Thus, this quasi-SSRGT orbit will coincide with its SSRGT counterpart every 40 days in terms of both solar illumination and ground location. All feasible solutions with a 40-day period are depicted in **Figure 7**(B). **Figure 8** summarizes how this synchronization is achieved for positive and negative $\Delta\omega_E$ values. Although the synchronization period is rather long, low-inclination quasi-SSOs provide more observation opportunities than high-inclination orbits for equatorial regions, and their satellite imagery taken from varied view angle may be useful for multi-angular Earth remote sensing[24].

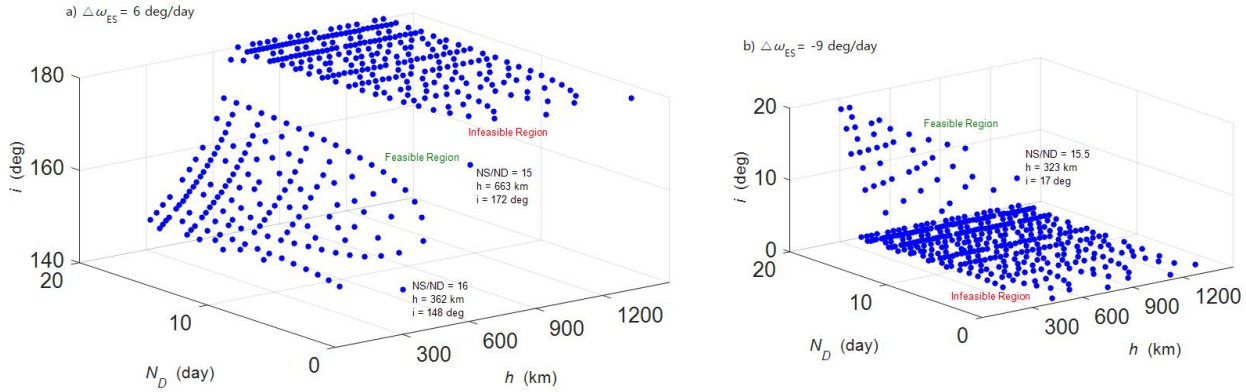

Figure 7. Inclination and altitude of quasi-SSOs with varied RGT ratios when (A) $\Delta\omega_{ES}$ = 6 deg/day and (B) $\Delta\omega_{ES}$ = -9 deg/day.

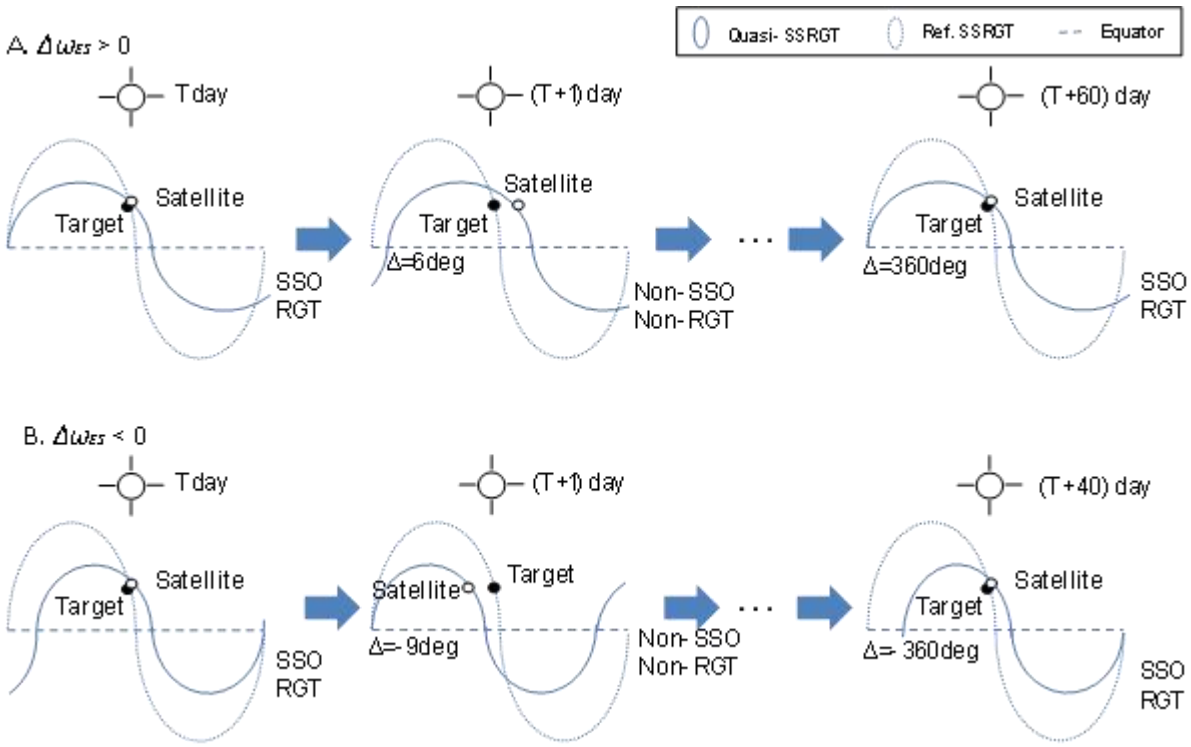

Figure 8. Quasi-synchronization of quasi-SSOs with their corresponding reference SSOs.

4.2 Tidal-synchronous Orbits

Besides the Sun, the Moon is another celestial body that exerts considerable gravitational forces on the Earth, creating lunar tides. The bio-optical reflectance of coastal waters depends on the local hydrographic features and phytoplankton composition, whose changes are attributable to lunar tides[25–27]. Satellite remote sensing provides the only avenue by which marine primary production (phytoplankton) can be studied at both oceanic and regional scales[26,28]. If the ocean color data is captured at regular, known tidal states, comparisons between equivalent data can be done without relative errors or complicated validation methods to correct them. Tidal synchronous orbits (TSOs) can be defined in a similar way to Sun-synchronous orbits. Equation (10) for the inclination and altitude of TSOs is obtained by substituting the Earth's spin rate ω_E in Eq. (3) with the Moon's rotation rate around the Earth ω_{EM}. The Moon's revolution period (i.e. one tidal lunar day) is $2\pi/\omega_{EM}$ = 24h 50m 8s which is slightly longer than one Earth sidereal day equal to $2\pi/\omega_E$ = 23h 56m 4s. This is because the Moon orbits around the Earth in the identical direction the Earth spins. A tidal lunar day is the minimum time period which can describe periodicity of all tidal types: semi-diurnal, diurnal and mixed. Equation (10) also shows that the lunar repeat ratio τ_L is defined using the lunar nodal period T_L and the number of lunar revolutions N_L.

$$\tau_L = \frac{N_S}{N_L} = \frac{T_L}{T_S} = \frac{2\pi/(\omega_{EM}-\dot{\Omega})}{2\pi/(\dot{M}+\dot{\omega})} = \frac{\dot{M}+\dot{\omega}}{\omega_{EM}-\dot{\Omega}} \quad (10)$$

Because the Earth's spin rate is replaced with the Moon's rotation rate in this formulation, a TSO cannot have RGTs by nature. However, one can define a metric of measuring how close a TSO is to an SSRGT orbit. One possible criterion is the annual drift in right ascension of ascending node (RAAN). Because the RAAN of an SSRGT drifts by 360 degrees (2π radians) a year, the closer a TSO's annual RAAN regression is to 2π, the more it is "SSRGT-like." This means that $\Delta\Omega_{year} = |\ 2\pi - d\Omega/dt \times T_{year}|$ is minimized or falls below a tolerance value. For example, N_L = 57 and N_S = 885 achieves a TSO in which a satellite completes 885 orbital revolutions every 57 tidal cycles[29]; the satellite will return to a new location with the same tidal conditions, but the new location will geographically differ from the old location. It is analogous to an SSO which does not have RGTs. First, if the TSO has an inclination of 97.6°, its annual RAAN drift will be 355°/year, differing by only 5°/year compared to an SSO. An inclination of 97.6° is chosen because it is the inclination of a τ = 15 SSRGT orbit in **Figure 5**(A). The TSO with this inclination is a SSRGT-like, neither an SSO nor an RGT orbit, but close. It can also be said, from the

other perspective, that this SSRGT orbit is TSO-like. Second, if the TSO with the same N_L and N_S values use an inclination of 97.7°, the annual RAAN drift becomes 360°/year. This inclination and the corresponding altitude (574 km) can be obtained by replacing $d\Omega/dt$ with ω_{ES} in Eq. (10). This orbit does not have RGTs anymore, not synchronized with Earth spin, but achieves synchronization with the Moon and the Sun at the same time. This "Tidal-Sun-synchronous" orbit (TSSO) incorporates lunar-solar dual-synchronization characteristics, which can already be witnessed in nature as spring tides and neap tides. This kind of orbits may be applicable to oceanography research as well as quantum satellite communications in which background noises from the Sun and the Moon must be controlled[30].

5. Conclusion

This paper surveyed a variety of satellite orbits for Earth remote sensing and proposed new types of orbits. First, a basic theory behind Sun-synchronous orbits (SSOs) is explained, which has been the most popular orbit to date. The A-train (Afternoon Train) constellation is an excellent example where SSOs are used by Earth observation satellites with different purposes, namely studying cloud physics (CloudSat, PARASOL, CALIPSO), water cycles (Aqua) and climate changes (OCO-2, GCOM-W1).

Another useful orbit property is a repeat ground track (RGT). An SSO is usually designed to also have an RGT such that satellites will fly over the same geographical locations under consistent surface lighting conditions. It is possible, however, for an SSO to adopt a non-repeating ground track by design such that the satellite path will move at a similar speed with moving targets. With drift ground tracks, mobile targets in the ocean and atmosphere such as glaciers and typhoons may be observed.

There are also possible variants of Sun-synchronous repeat ground track (SSRGT) orbits. A quasi-SSRGT orbit coincides with an SSRGT orbit periodically. An SSRGT-like orbit does not periodically coincide with an SSRGT orbit but shares similar orbital characteristics. In lieu of the Earth's revolution around the Sun, an orbit can also be with synchronized with the Moon's revolutions around the Earth, resulting in a lunar tidal synchronous orbit (TSO) which has potential applications in oceanography research.

Although the understanding of orbital characteristics helps to make use of satellite data, it should be taken into account from early mission design stages. Miniaturization of satellites and emergence of large satellite constellations are promoting the affordability of Earth remote sensing through economies of scale. Although Earth observations in microwave frequencies (radio spectrum above 1GHz and below 300GHz for far-infrared waves) do not usually require Sun synchronization, they may still use SSOs for multi-spectral sensing and data integration as demonstrated by CloudSat which is part of the A-train constellation. There may be other types of satellite orbits preferred for microwaves or GPS signals, which is another topic of research.

Conflict of Interest

No conflict of interest was reported by the authors.

Acknowledgments

The authors thank the anonymous reviewers for their constructive comments.

References

1. Loveland TR, Dwyer JD. Landsat: Building a strong future. Remote Sensing of Environment 2012; 122: 22–29.
2. Fu LL, Holt B. Satellite views oceans and sea ice with synthetic-aperture radar. Jet Prolusion Laboratory Publication 1982; 81–120: 200pp.
3. Logan T, Holt B, Drew L. The newest oldest data from SeaSat's synthetic aperture radar. EOS Transactions of American Geophysical Union 2014; 95(11): 93–100.
4. McCormick MP, Zawodny JM, Veiga RE, *et al*. An overview of sage I and II ozone measurements. Planetary and Space Science 1989; 37(12): 1567–1586.
5. L'Ecuyer TS, Jiang JH. (2011). Touring the atmosphere aboard the A-train. AIP Conference Proceedings 2011; 1401(1): 22–29.
6. Parkinson CL. Aqua: An Earth-observing satellite mission to examine water and other climate variables. IEEE Transactions on Geoscience and Remote Sensing 2003; 41(2): 173–183.
7. Stephens LS, Vane DG, Tanelli S, *et al*. CloudSat mission: performance and early science after the first year of operation. Journal of Geophysical Research: Atmospheres 2008; 113(D8): 18pp.

8. Short NM, Stoney W, Rosalanka J, *et al*. The remote sensing tutorial. NASA Goddard Space Flight Center 2004.
9. Ruf C, Atlas R, Chang PS, *et al*. New ocean winds satellite mission to probe hurricanes and tropical convection. Bulletin American Meteorological Society 2016.
10. Scharroo R, Bonekamp H, Ponsard C, *et al*. Jason continuity of services: continuing the Jason altimeter data records as Copernicus Sentinel-6. Ocean Science 2016; 12: 471–479.
11. Boain, RJ. A-B-Cs of Sun-Synchronous Orbit Mission Design. AAS/AIAA Space Flight Mechanics Conference Proceedings 2004; 04–108: 19pp.
12. Heynderickx D. Radiation belt modeling in the framework of space weather effects and forecasting. Journal of Atmospheric and Solar-Terrestrial Physics 2004; 64(16): 1687–1700.
13. Vallado DA. Fundamentals of Astrodynamics and Applications, 3rd Edition, New York 2007.
14. Paek SW. Reconfigurable satellite constellations for geo-spatially adaptive Earth observation missions. Massachusetts Insittute of Technology 2012; 155pp.
15. Paek SW, de Weck OL, Smith MW. (2017). Concurrent design optimization of Earth observation satellites and reconfigurable constellations. Journal of the British Interplnetary Soceity 2017; 70(1): 18pp.
16. Kronig L, Paek SW, Ivanov A, *et al*. Satellite constellation design for the SOLVE mission investigating diurnal cycles of vegetation phenomena. AAS Space Flight Mechanics Meeting Proceedings 2016; 18pp.
17. Paek SW, de Weck OL. Greening Earth from Space – Turning Deserts into Forests with Space Solar Power. Journal of the British Interplnetary Soceity 2017; 70(1): 9pp.
18. Paek SW. A delta-v map of useful orbits for Earth observation missions. Proceedings of the International Astronautical Congress, IAC 2014; 8pp.
19. Carter, D. When is the Groundtrack drift rate zero? Charles Stark Draper Laboratory Memorandum 1991; ESD- 91–020.
20. Dorst, N. (2014). What is the average forward speed of a hurricane? [online database]. URL: http://www.aoml.noaa.gov/hrd/tcfaq/G16.html [cited 4 May 2018]
21. Blackwell WJ, Allen G, Conrad S, *et al*. Nanosatellites or Earth Environmental Monitoring: The MicroMAS Project. AIAA/USU Conference on Small Satellites Proceedings 2012; 8pp.
22. Blackwell WJ, Allen G, Galbraith C, *et al*. MicroMAS: A First Step Towards a Nanosatellite Constellation for Global Storm. AIAA/USU Conference on Small Satellites Proceedings 2013; 10pp.
23. Bruccoleri C, Wilkins MP, Mortari D. On Sun-Synchronous Orbits and Associated Constellations. Dynamics and Control of Systems and Structures in Space Conference Proceedings 2004.
24. Nag S, Gatebe CK, Miller DW, *et al*. Effect of Satellite Formations and Imaging Modes on Global Albedo Estimation. Acta Astronautica 2016; 126: 77–97.
25. Balch WM. An apparent lunar tidal cycle of phytoplankton blooming and community succession in the Gulf of Maine. Journal of Experimental Marine Biology and Ecology 1981; 55(1): 65–77.
26. Hoepffner N, Sathyendranath S. Bio-optical characteristics of coastal waters: Absorption spectra of phytoplankton and pigment distribution in the western North Atlantic. Limnology and Oceanography 1992; 37(8): 1660–1679.
27. Platt T, Sathyendranath S. Oceanic primary production: estimation by remote sensing at local and regional scales. Science 1988; 241(4873): 1613–1620.
28. Ahn YH, Shanmugam P. Detecting the red tide algal blooms from satellite ocean color observations in optically complex Northeast-Asia. Remote Sensing of Environment 2006; 103(4): 419–437.
29. Lowe C, Macdonald M, Greenland S, *et al*. 'Charybdis'–The Next Generation in Ocean Colour and Biogeochemical Remote Sensing. AIAA/USU Conference on Small Satellites Proceedings 2012.
30. Bourgoin JP, Meyer-Scott E, Higgins BL, *et al*. A comprehensive design and performance analysis of low Earth orbit satellite quantum communication. New Journal of Physics 2013; 15(023006): 39pp.